Supplementary Information (SI) for ChemComm.

Supplementary Information

Triethyl methyl ammonium ionic liquid as effective electrolyte additive for high-performance zinc-iodine batteries

Xin Wu,[ab] Wei Wei,[c] Xue Yang,*[b] Le Yu,*[ab] and Xiao Chun Chen*[b]

[a]State Key Lab of Organic-Inorganic Composites, Beijing University of Chemical Technology, Beijing 100029, P.R. China

[b]College of Chemical Engineering, Beijing University of Chemical Technology, Beijing 100029, P.R. China

[c]China National Building Material Test & Certification Group Co., Ltd.

E-mail: yangx@buct.edu.cn; yule@mail.buct.edu.cn; chenxc@mail.buct.edu.cn

Experimental Section

Chemicals

Multi-walled Carbon nanotubes were purchased from TCI (Shanghai) Development Co., Ltd. Single-walled Carbon nanotubes were purchased from Macklin. Triethyl methyl ammonium chloride ($N_{2221}Cl$) and $ZnSO_4 \cdot 7H_2O$ were obtained from Aladdin. The titanium mesh was acquired from Taobao. ZnI_2 was obtained from Innochem Technology Co., Ltd.

Electrolyte preparation

Add 5.75 mg of $ZnSO_4 \cdot 7H_2O$ into a 10 mL volumetric flask, then dilute to the mark with water to prepare a 0.2 M $ZnSO_4$ electrolyte. Ionic liquid-based electrolytes were prepared by adding 5.75 mg of $ZnSO_4 \cdot 7H_2O$ and different amounts of $N_{2221}Cl$ to a 10 mL volumetric flask, then diluting to the mark with water. When the amounts of $N_{2221}Cl$ were 0.30 mg, 0.76 mg, or 1.51 mg, 2 M $ZnSO_4$ + 0.2 M $N_{2221}Cl$, 2 M $ZnSO_4$ + 0.5 M $N_{2221}Cl$ and 2 M $ZnSO_4$ + 1 M $N_{2221}Cl$ electrolytes were obtained, respectively.

Cathode preparation

A piece of titanium (Ti) mesh (40 mm × 10 mm) was cut as a support. 320 mg of multi-walled carbon nanotubes and 80 mg of single-walled carbon nanotubes were thoroughly mixed. Then, 71.6 μL of PTFE slurry and a certain amount of isopropanol were added to the mixture and uniformly ground until a ‘wet dough’ of suitable viscosity was obtained. The dough was placed in a roller press and rolled several times to form a homogeneous, crack-free film. The film was placed on a Ti mesh and rolled again in the roller press to ensure that the film adhered firmly to the Ti mesh. The thickness of the roller press was set to 200 μm, and then the electrodes were dried at 80°C to remove the remaining isopropanol to obtain carbon nanotube (CNT) membrane electrode sheets. The electrode sheet was cut into a disc shape with a diameter of 10 mm. A certain amount of ZnI_2 was weighed and dissolved in ethanol, and the prepared ZnI_2-ethanol solution was uniformly dripped onto the electrode sheet. The sheet was then placed in a vacuum oven and dried at 60 °C for 12 h to obtain the positive electrode sheet. The loading of ZnI_2 on the CNT electrode (denoted as CNT-ZnI_2) was about 12 mg cm^{-2}.

Material characterizations

Raman test was obtained by inVia Reflex Raman spectrometer. Valence states were analyzed by X-ray photoelectron spectroscopy (XPS; ESCALAB 250). Surface morphology was examined by field-emission scanning electron microscope (FESEM; TESCAN Clara; JEOL JSM-7800F). Ionic conductivity of the electrolyte was tested by a conductivity meter (DDS-307A). Ultraviolet-visible spectroscopy (UV-Vis; UV-2501PC) was used to examine the I_3^- ions in the electrolyte.

Electrochemical measurements

Both of Zn foil and CNT-ZnI_2 electrode were cut into discs with a diameter of 10 mm. Cycling and rate performance were investigated on a Neware battery tester using CR2032 coin cells with CNT-ZnI_2 as the working electrode, glass fiber membrane as the separator, and Zn foil as the counter electrode. Cyclic voltammetry (CV) tests were carried out using an electrochemical workstation (IviumStat). Electrochemical impedance spectroscopy measurements were carried out on Autolab electrochemical workstation over the frequency from 0.1 Hz to 100 kHz with an amplitude of 10 mV.

Zn^{2+} ion transference number ($t_{Zn^{2+}}$) was determined by the following equation:

$$t_{Zn^{2+}} = \frac{I_s(\Delta V - I_0R_0)}{I_0(\Delta V - I_sR_s)}$$

where ΔV was the constant polarization voltage applied (10 mV), I_0 and R_0 were the initial current and resistance, respectively, and I_s and R_s were the steady-state current and resistance.

First, Zn was deposited on the copper foil at a capacity of 5 mAh cm^{-2} and then Zn was stripped off at a cut-off voltage of 0.5 V. Then, Zn with a capacity of 5 mAh cm^{-2} (Q_r) was deposited on the copper foil at 0.5 mAh cm^{-2}. Subsequently, Zn stripping/deposition was performed 9 times (n) at a current density of 0.5 mA cm^{-2} and a surface capacity of 1 mAh cm^{-2} (Q_c). Finally, the capacity (Q_s) was obtained when charged to 0.5 V. The Coulombic efficiency (CE) for Zn deposition/stripping were calculated by following equation:

$$\mathrm{CE_{ave}} = \frac{nQ_\mathrm{c} + \mathrm{Q_s}}{n\mathrm{Q_c} + \mathrm{Q_r}}$$

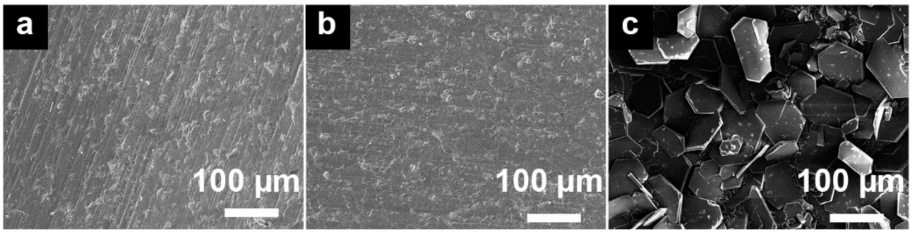

Fig. S1. FESEM images of (a) pristine Zn foil and Zn foils soaked in (b) 2 M $ZnSO_4$ + 0.5 M $N_{2221}Cl$ and (c) 2 M $ZnSO_4$ for 15 days.

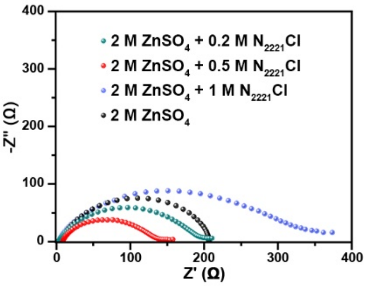

Fig. S2. Nyquist plots of Zn-Zn symmetric cells based on different electrolytes.

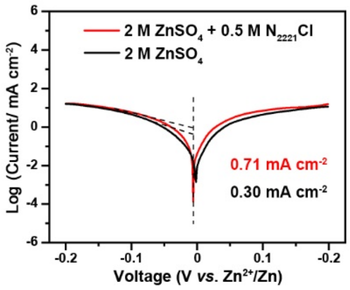

Fig. S3. Tafel curves of Zn electrodes in different electrolytes.

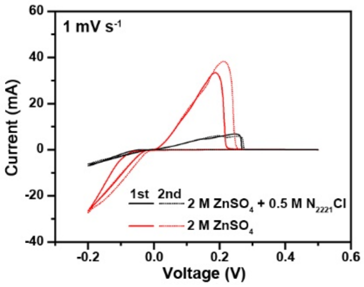

Fig. S4. CV curves of Cu-Zn cells based on different electrolytes at a scan rate of 1 mV s^{-1}.

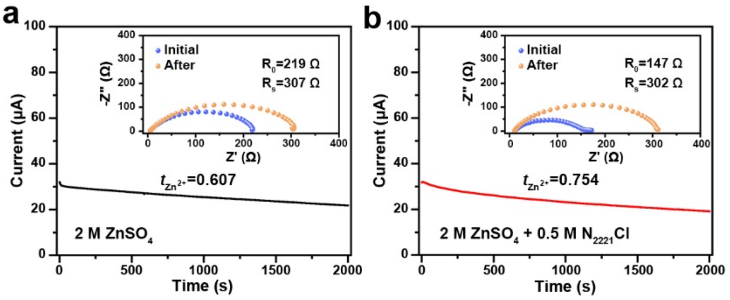

Fig. S5. Current-time plots of (a) 2 M $ZnSO_4$ and (b) 2 M $ZnSO_4$ + 0.5 M $N_{2221}Cl$ in Zn-Zn cell at a constant potential of 10 m V. Insert: Nyquist plots before and after polarization.

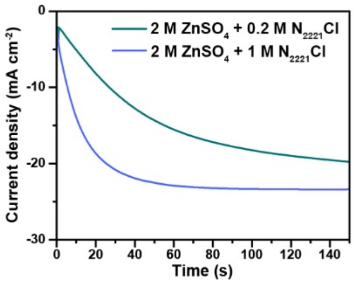

Fig. S6. CA curves at a constant overpotential of -150 mV.

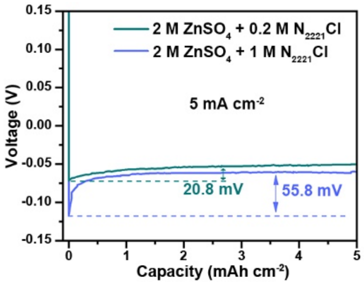

Fig. S7. Chronopotentiometry curves of Cu-Zn cells using different electrolytes.

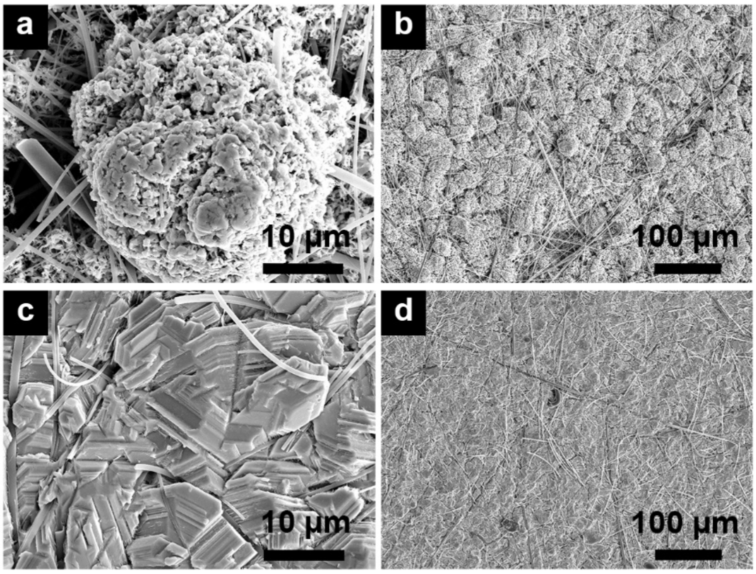

Fig. S8. FESEM images of the deposited Zn with a capacity of 10 mAh cm^{-2} in (a, b) 2 M $ZnSO_4$ and (c, d) 2 M $ZnSO_4$ + 0.5 M $N_{2221}Cl$.

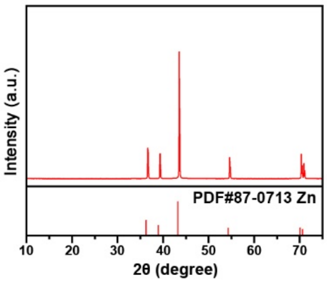

Fig. S9. XRD pattern of Zn foil after cycling in 2 M $ZnSO_4$ + 0.5 M $N_{2221}Cl$.

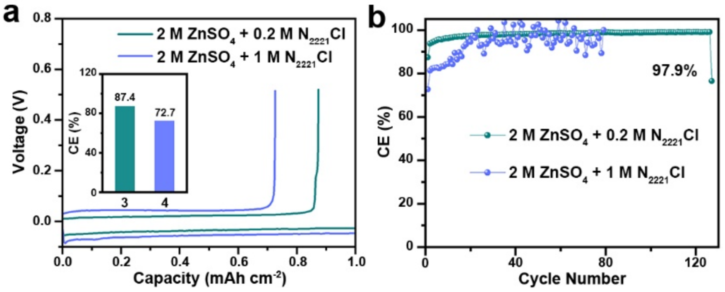

Fig. S10. (a) Plating/stripping profiles and initial CEs and (b) CE plots of Cu-Zn cells.

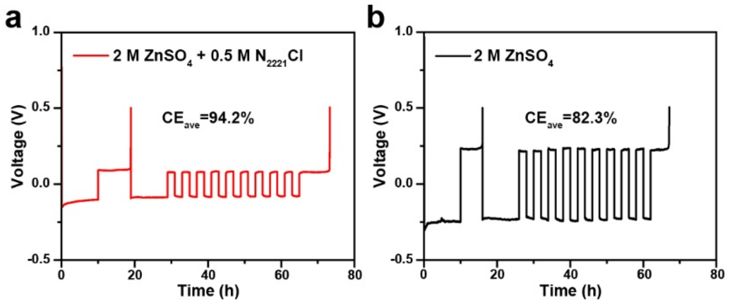

Fig. S11. Voltage-time curves of Cu-Zn cells using (a) 2 M $ZnSO_4$ + 0.5 M $N_{2221}Cl$ and (b) 2 M $ZnSO_4$ electrolyte.

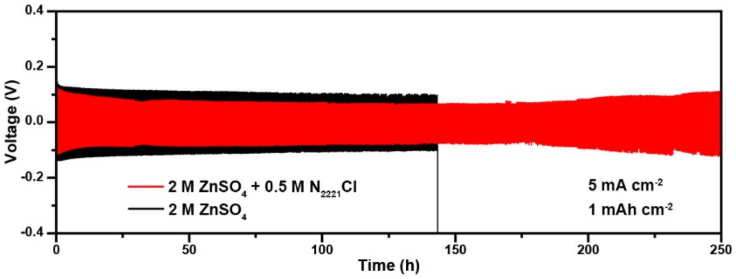

Fig. S12. Cycling performance of Zn-Zn batteries using different electrolytes.

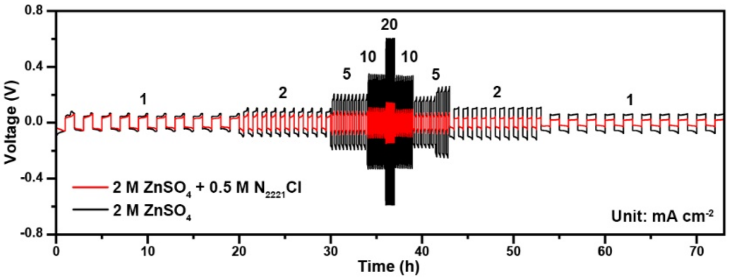

Fig. S13. Rate performance of Zn-Zn batteries using different electrolytes.

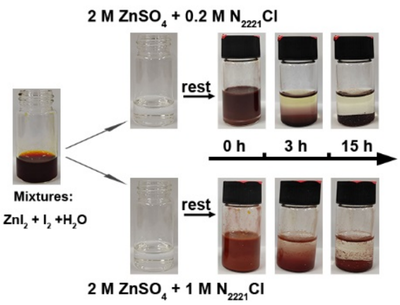

Fig. S14. Optical images of the electrolyte resting for different times after adding a mixture of triiodide.

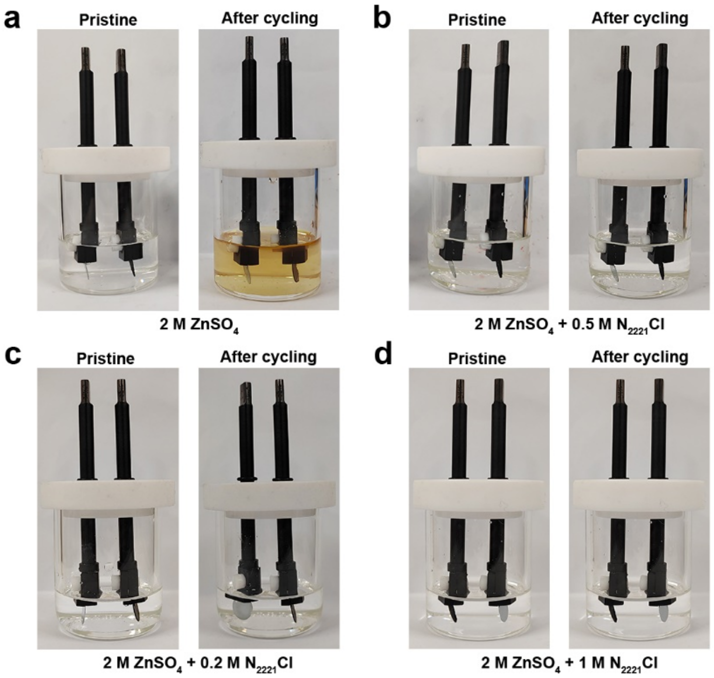

Fig. S15. Optical images after the charging of ZIBs with CNT-ZnI$_2$ cathode using (a) 2 M ZnSO$_4$, (b) 2 M ZnSO$_4$ + 0.5 M N$_{2221}$Cl, (c) 2 M ZnSO$_4$ + 0.2 M N$_{2221}$Cl, and (d) 2 M ZnSO$_4$ + 1 M N$_{2221}$Cl.

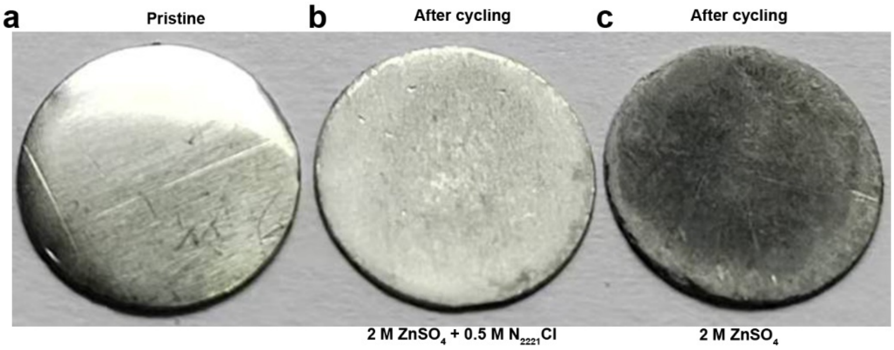

Fig. S16. Optical images of (a) pristine Zn anode and the Zn anodes after cycling in ZIBs using (b) 2 M $ZnSO_4$ + 0.5 M $N_{2221}Cl$ and (c) 2 M $ZnSO_4$ electrolytes.

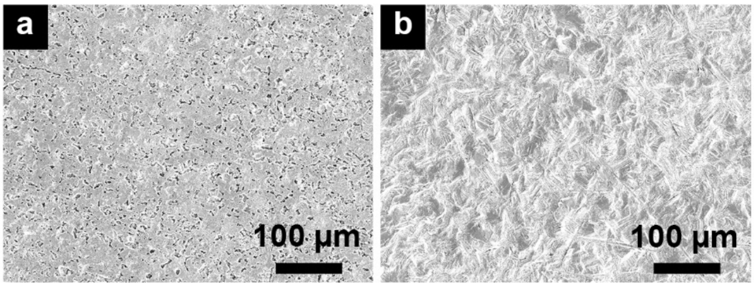

Fig. S17. FESEM images of Zn anodes after cycling in (a) 2 M $ZnSO_4$ and (b) 2 M $ZnSO_4$ + 0.5 M $N_{2221}Cl$.

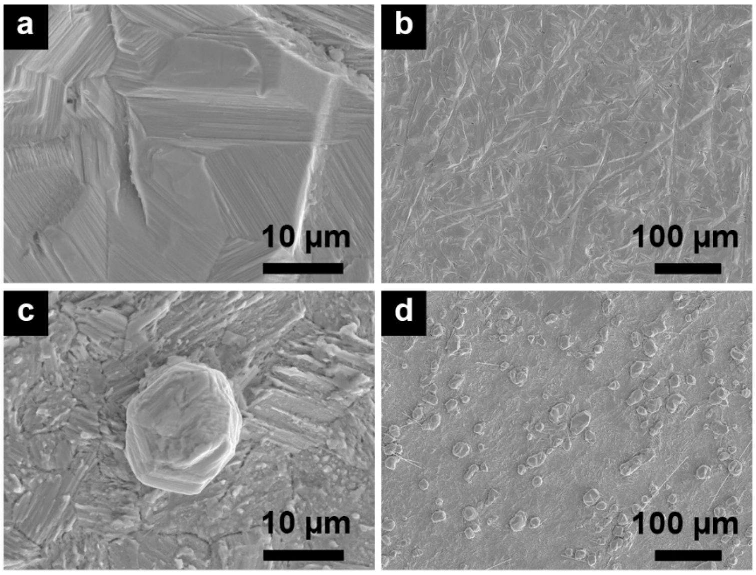

Fig. S18. FESEM images of Zn anodes after cycling in (a, b) 2 M $ZnSO_4$ + 0.2 M $N_{2221}Cl$ and (c, d) 2 M $ZnSO_4$ + 1 M $N_{2221}Cl$.

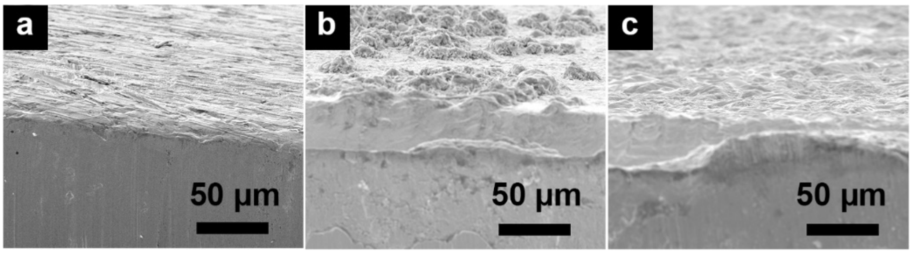

Fig. S19. Cross-sectional FESEM images of (a) pristine Zn anode, Zn anodes after cycling in ZIBs using (b) 2 M $ZnSO_4$ and (c) 2 M $ZnSO_4$ + 0.5 M $N_{2221}Cl$ electrolytes.

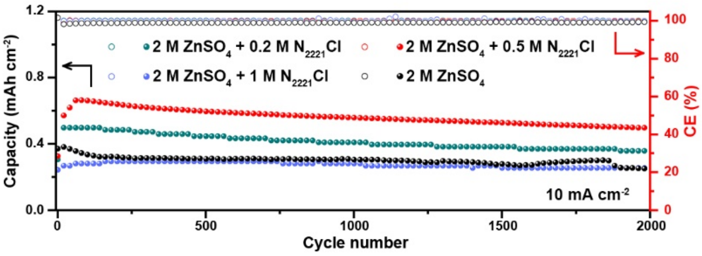

Fig. S20. Cycling performance of ZIBs with different amounts of $N_{2221}Cl$ as electrolyte additives.

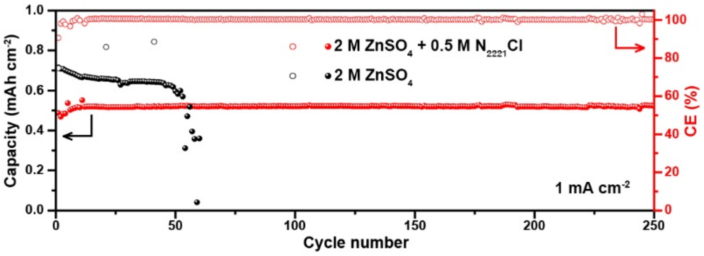

Fig. S21. Cycling performance of ZIBs using 2 M $ZnSO_4$ + 0.5 M $N_{2221}Cl$ electrolyte and 2 M $ZnSO_4$.

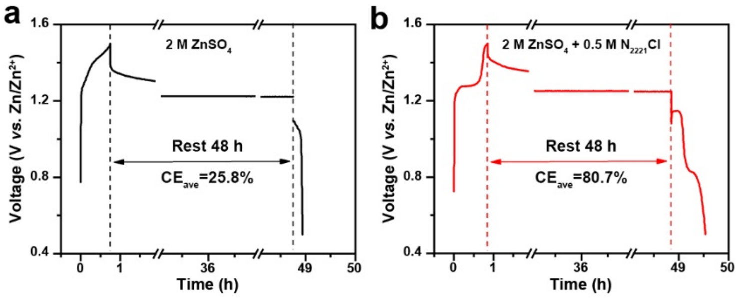

Fig. S22. Self-discharging voltage profiles of ZIBs using (a) 2 M $ZnSO_4$, and (b) 2 M $ZnSO_4$ + 0.5 M $N_{2221}Cl$ electrolyte.

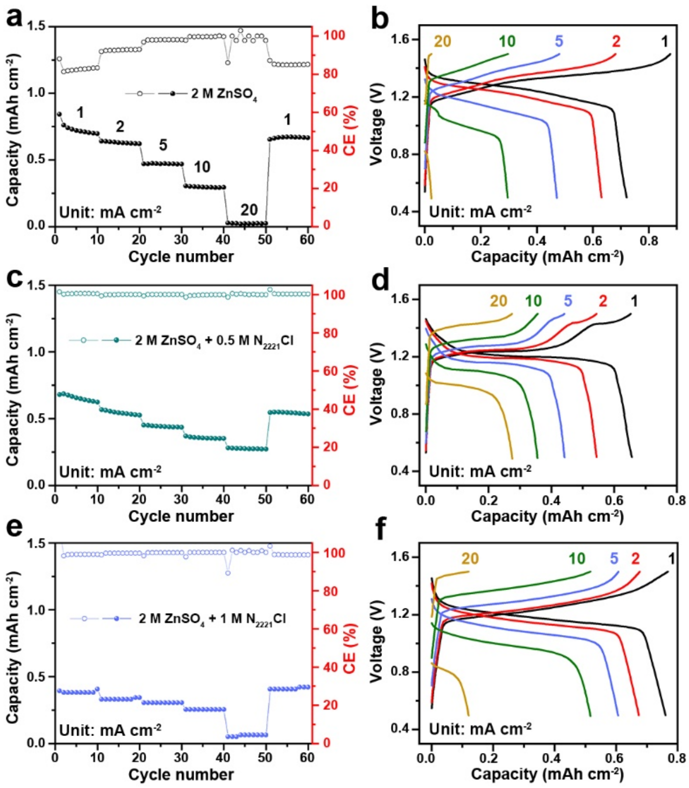

Fig. S23. (a, c, e) Rate performance of ZIBs and (b, d, f) the corresponding galvanostatic charge-discharge curves using a, b) 2 M $ZnSO_4$, c, d) 2 M $ZnSO_4$ + 0.2 M $N_{2221}Cl$, and e, f) 2 M $ZnSO_4$ + 1 M $N_{2221}Cl$.

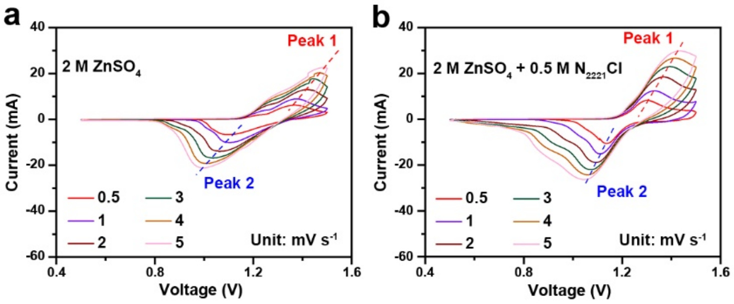

Fig. S24. CV curves of ZIBs using (a) 2 M $ZnSO_4$ and (b) 2 M $ZnSO_4$ + 0.5 M $N_{2221}Cl$ electrolyte at different scan rates.

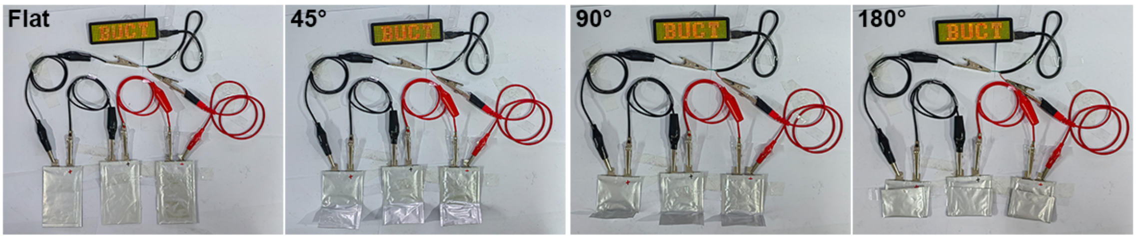

Fig. S25. Flexibility tests of pouch cells using 2 M $ZnSO_4$ + 0.5 M $N_{2221}Cl$ electrolyte under different bending conditions.

Table S1. Ionic conductivity of various electrolytes at 20℃.

Electrolytes	0.2 M $N_{2221}Cl$	0.5 M $N_{2221}Cl$	1 M $N_{2221}Cl$	$ZnSO_4$
Ionic conductivity (mS cm^{-1})	53.4	49.0	37.4	55.6

Table S2. pH values of various electrolytes at 20℃.

Electrolyte	0.2 M $N_{2221}Cl$	0.5 M $N_{2221}Cl$	1 M $N_{2221}Cl$	$ZnSO_4$
pH value	3.89	3.91	4.00	3.86

Table S3. Caparison of the electrochemical performance of ZIBs with previous related publications.

Cathode	Electrolyte	Cycling stability	Ref.
$AC@I_2$	Zn-ML	85.2% after 3000 cycles at 0.5 A g^{-1} 80.7% after 2100 cycles at 1 A g^{-1}	S1
MnFn-PBA/I_2	2 M $ZnSO_4$	76.0% after 1200 cycles at 0.5 A g^{-1}	S2
$AC@I_2$ with LA133 binder	0.5 M $ZnSO_4$ + 0.5 M Li_2SO_4	83.3% after 1000 cycles at 2 A g^{-1}	S3
Ni-N_4CNF/I_2	2 M $ZnSO_4$	74% after 5900 cycles at 3 A g^{-1}	S4
SPAN	Z/I_2/G4	81.8% after 800 cycles at 2 A g^{-1}	S5
$I_2@AC$	ZSO/SA-10	75.4% after 400 cycles at 1 A g^{-1}	S6
CNT-ZnI_2	2 M $ZnSO_4$ + 0.5 M $N_{2221}Cl$	89.8% after 2000 cycles at 2 A g^{-1} 74.7% after 2000 cycles at 1 A g^{-1}	this work

Supplementary references

S1 F. L. Li, C. C. Zhou, J. Zhang, Y. T. Gao, Q. Nan, J. M. Luo, Z. M. Xu, Z. J. Zhao, P. Rao, J. Li, Z. Y. Kang, X. D. Shi and X. L. Tian, *Adv. Mater.*, 2024, **36**, 2408213.

S2 Y. Qian, G. Chang, C. Huang, Y. J. Yang, Y. S. Hao, Q. L. Tang, A. P. Hu, Y. H. Li and X. H. Chen, *Chem. Eng. J.*, 2025, **503**, 158392.

S3 K. Wang, H. Li, Z. Xu, Y. Liu, M. Ge, H. Wang, H. Zhang, Y. Lu, J. Liu, Y. Zhang, Y. Tang and S. Chen, *Adv. Energy Mater.*, 2024, **14**, 2304110.

S4 W. T. Qu, J. Zhu, G. Z. Cao, S. L. Chen, Y. W. Tan, B. H. Chen and M. Zhang, *Small*, 2024, **20**, 2310475.

S5 H. Li, M. T. Zhang, Z. Y. Zheng, X. R. Wu, X. Xiao, Z. H. Piao, C. Li, Y. Y. Jia, J. L. Yang and G. M. Zhou, *Adv. Mater.*, 2025, **37**, 2409771.

S6 Q. T. Chen, K. F. Ouyang, Y. Y. Wang, M. F. Chen, H. W. Mi, J. Z. Chen, C. X. He, H. Li, D. T. Ma and P. X. Zhang, *Adv. Funct. Mater.*, 2024, **34**, 2406386.